

FULL PAPER

Open Access



# Comparison of three retrievals of COSMIC GPS radio occultation results in the tropical upper troposphere and lower stratosphere

Noersomadi<sup>1,2\*</sup>  and Toshitaka Tsuda<sup>1,3</sup> 

## Abstract

Combining geometrical optics (GO) and wave optics (WO), the COSMIC data analysis and archive center (CDAAC) retrieved two sets of dry atmosphere temperatures ( $T$ ) from COSMIC GPS radio occultation (GPS-RO), which are called atmPrf2010 and atmPrf2013. In atmPrf2010, the sewing height between WO and GO varies between 10 and 20 km, but is fixed at 20 km for atmPrf2013. The height resolution of the atmPrf2010 depends on the sewing height, while the  $T$  profiles by atmPrf2013 are smoothed over 500 m. We also derived  $T$  by applying WO throughout the troposphere and the stratosphere up to a 30-km altitude, which is called rishfsi2013. The three retrievals have different characteristics in the height resolution around the tropopause. Therefore, we aim to examine a possible discrepancy in the statistical results of the cold-point tropopause (CPT) and the lapse rate tropopause (LRT) among the three datasets, conducting their inter-comparisons as well as the comparison between GPS-RO and the simultaneous radiosonde dataset. We investigate the  $T$  variations in the upper troposphere and lower stratosphere (UTLS) over the tropics from October 1, 2011, to March 31, 2012, when radiosonde soundings were conducted as the CINDY-DYNAMO 2011 campaign. The mean  $T$  profiles are consistent between atmPrf2010 and atmPrf2013, but rishfsi2013 results are colder (warmer) than the CDAAC retrievals below (above) the tropopause. The mean  $T$  difference between atmPrf2013 and atmPrf2010 is 0.17 K at the cold-point tropopause (CPT) and  $-0.38$  K at the lapse rate tropopause (LRT). On the other hand, rishfsi2013 shows a colder  $T$  at CPT by  $-0.77$  and  $-0.59$  K relative to atmPrf2013 and atmPrf2010, respectively, and the warmer  $T$  by 0.60 and 0.20 Kd at LRT. During CINDY-DYNAMO, we found 134 radiosonde soundings that coincide with GPS-RO within  $\pm 3$  h and are collocated within 200 km from GPS-RO. The mean  $T$  difference at CPT from the radiosondes is 0.32, 0.49 and  $-0.24$  K for atmPrf2010, atmPrf2013 and rishfsi2013, respectively. Both atmPrf2013 and atmPrf2010 have a positive bias at CPT, while rishfsi2013 has a negative one. Similar comparisons at LRT are  $-0.45$ ,  $-0.69$  and  $-0.41$  K, respectively, showing a negative bias for all GPS-RO retrievals. The results show that rishfsi2013 is consistent with the retrievals at CDAAC and the radiosondes. Due to its good height resolution, rishfsi2013 is useful for studies on mesoscale  $T$  perturbations in the UTLS.

**Keywords:** COSMIC, GPS radio occultation (GPS-RO), Full spectrum inversion (FSI), Upper troposphere–lower stratosphere (UTLS), Retrieval algorithm

\*Correspondence: noersomadi@lapan.go.id

<sup>1</sup> Research Institute for Sustainable Humanosphere (RISH), Kyoto University, Kyoto, Japan

Full list of author information is available at the end of the article

## Introduction

The global positioning system radio occultation (GPS-RO) technique is an active limb sounding of the Earth's atmosphere and ionosphere using the characteristics of microwave propagation from GPS satellites at an orbit altitude of 20,200 km to the low-Earth-orbit (LEO) satellites around 700 km (Ware et al. 1996). In April 2006, the University Corporation for Atmospheric Research (UCAR) and the National Space Organization (NSPO) of Taiwan jointly conducted a very successful GPS-RO mission, called the Constellation Observing System for Meteorology, Ionosphere, and Climate (COSMIC), consisting of six LEO satellites (Anthes et al. 2008). The GPS-RO has produced highly accurate atmospheric profiles, significantly improving the weather forecasting performance and providing long-term stable references for climate applications (e.g., Anthes 2011; Ladstädter et al. 2015). In addition, GPS-RO temperature profiles with superior height resolutions provide a unique opportunity to study the mesoscale temperature fluctuations caused by atmospheric waves in the stratosphere (Alexander et al. 2008; Tsuda et al. 2011), and analysis of internal gravity wave parameters (Gubenko et al. 2011).

The fundamental retrieval techniques for the GPS-RO data are geometric optics (GO) and wave optics (WO), assuming that the atmosphere has spherical symmetry (Melbourne 2004). The GO method constructs the L1 and L2 bending angles in the neutral atmosphere by the time derivative of the excess phase (Doppler) and the positions and velocities of the GPS and LEO satellites (Kuo et al. 2004). To reduce the influence of the ionosphere, optimal filtering is applied on the L2 bending angle. Then, the ionospheric-free bending angle is obtained by combining the L1 and L2 bending angles (Sokolovskiy et al. 2009; Schreiner et al. 2011). The vertical resolution of the GO profile is limited to about 1.4 km by the Fresnel zone (Kursinski et al. 1997).

In the lower atmosphere, where GO cannot solve the multipath problem caused by sharp vertical moisture gradients, the WO method is used by applying integral transforms to the entire raw phase and complex amplitude signals to derive the L1 bending angle. Typical WO methods are canonical transform (CT) (Gorbunov 2002; Gorbunov and Lauritsen 2004), full spectrum inversion (FSI) (Jensen et al. 2003) and phase matching (PM) (Jensen et al. 2004), which provide a good vertical resolution of about 0.1–0.3 km. The entire ionosphere-free bending angle profile is, then, obtained by combining (sewing) the GO and WO profiles (Kuo et al. 2004; Schreiner et al. 2011).

The Abel inversion is applied to derive the refractive index profile from the ionosphere-free bending angles. The dry atmospheric temperature ( $T$ ) can be directly

obtained by neglecting the effects of water vapor pressure on the refractive index and assuming a hydrostatic equilibrium and the ideal gas law. The  $T$  profiles significantly differ from the real temperature below about 6 and 10 km at high and low latitudes, respectively (Scherllin-Pirscher et al. 2011). Because the neutral atmospheric bending angle decreases exponentially with height, the retrieved profiles above about 40 km may contain measurement errors due to ionospheric noise.

Tropopause fluctuations, which play an important role in the exchange mechanism between the troposphere and the stratosphere, influence global climate variations (Fueglistaler et al. 2009; Gettelman et al. 2011). The long-term GPS-RO data indicate climate change signals from warming in the upper troposphere and cooling in the lower stratosphere (Steiner et al. 2011). Many recent studies have utilized GPS-RO data to investigate the variability in the upper troposphere and the lower stratosphere (UTLS) such as fluctuation details of the cold-point tropopause (CPT) (Kim and Son 2012), and the occurrence of the multiple lapse rate tropopause (LRT) (Xu et al. 2014).

A multiple tropopause often appears in the equatorial region. Moreover, temperature variations near the tropical tropopause are more pronounced due to the effects of atmospheric waves. Thus, the detection of CPT and LRT may be affected by the height resolution of the  $T$  profile. Therefore, this issue needs to be considered when comparing CPT and LRT from the GPS-RO retrievals and radiosonde data.

The COSMIC data analysis and archive center (CDAAC) of UCAR published the COSMIC GPS-RO results in 2010 and 2013 using different retrieval algorithms. We also independently retrieved the COSMIC GPS-RO data. In this paper, we conduct a statistical comparison of the  $T$  variations in the tropical UTLS region among these three GPS-RO datasets. Additionally, we validate them by referring to simultaneous radiosonde data with an emphasis on the characteristics of the CPT and LRT.

“Data analysis” section outlines the three retrievals of the GPS-RO data, while “Results and discussion” section compares the  $T$  profiles in terms of the CPT and LRT among the three GPS-RO datasets. Finally, to validate the GPS-RO results, they are compared to the radiosondes.

## Data analysis

### COSMIC GPS-RO

CDAAC published Level 2 atmospheric dry profiles (atmPrf) in a height range up to 60 km from the ground. The first results were processed in 2006 and were reprocessed in 2009 (Sokolovskiy et al. 2009). Then in 2010, the atmPrf version 2010.2640 was published.

Wang et al. (2013) conducted a statistical test of the CDAAC atmospheric wet profiles (wetPrf) version 2010.2640. Compared to the global radiosonde data, a small bias of  $-0.09 \text{ K} \pm 1.72 \text{ K}$  was observed in the height range from 925 to 10 hPa. On the other hand, Das and Pan (2014) reported that the temperature differences between CDAAC wetPrf (wet) and atmPrf (dry) version 2010.2640 are nearly zero from 200 to 10 hPa. Although the dry temperature retrieval deviates from the real temperature in a moist atmosphere (Scherllin-Pirscher et al. 2011), the atmPrf version 2010.2640 is not affected by water vapor above about 10 km. This bias estimated by Wang et al. (2013) can also be applied as an index for the dry atmosphere.

The most common dataset is the updated version of atmPrf products published by CDAAC, which is known as 2013.3520. This study employs both atmPrf 2010.2640 and atmPrf 2013.3520, which are hereafter referred to as atmPrf2010 and atmPrf2013, respectively. Table 1 shows their fundamental characteristics. The retrieval in atmPrf2013 and atmPrf2010 adopts the PM and FSI methods, respectively, in the lower atmosphere. However, at higher altitudes, both adopt the GO method.

For atmPrf2010, the FSI method was employed up to a specified altitude between 10 and 20 km, depending on the ionospheric noise (Sokolovskiy et al. 2010; Schreiner et al. 2011). The sewing altitude, which is where FSI switches to GO, is prescribed for each atmPrf2010 profile. Consequently, the height for the transition of the vertical resolution varies in the UTLS region for individual GPS-RO events (Sokolovskiy et al. 2014).

For atmPrf2013, the sewing altitude from PM to GO is fixed at 20 km, producing a profile with the good height resolution up to 20 km. Height smoothing for altitudes between 10 and 20 km is applied to reduce the vertical resolution to 0.5 km, although the original height resolution of 0.1–0.3 km is kept below 10 km (Sokolovskiy et al. 2014).

Zeng et al. (2016) have suggested that in weather applications, the different dynamical extrapolation heights for each individual occultation profile, which is adopted in atmPrf2010, may be a better definition. However, for climate applications, it is better to fix the optimal transition

height from GO to WO at constant altitude (20 km) as applied in atmPrf2013.

We used the version 3520 data of COSMIC GPS-RO published by CDAAC, applying the same retrieval procedure and the background atmospheric model as in Tsuda et al. (2011). Hereafter, we call our results as rishfsi2013. The FSI software was coded at RISH with intensive support by CDAAC. We applied the FSI method up to 30 km with a vertical resolution of 0.1–0.2 km. Tsuda et al. (2011) reported that the FSI profile can be used to study mesoscale temperature perturbations such as atmospheric gravity waves with the upper limit about 28 km.

Figure 1 shows the total number of COSMIC GPS-RO profiles in the 10°S–10°N latitude range from October 1, 2011, to March 31, 2012. This period was selected considering the availability of the radiosonde data for comparison, which is introduced in the next subsection. Two different versions of COSMIC GPS-RO datasets by CDAAC as well as rishfsi2013 were processed. Compared to atmPrf2010 and rishfsi2013, atmPrf2013 has more atmospheric profiles; the totals are 12,760, 12,274 and 15,441, respectively. The difference in the number of retrieved profiles may be related to the truncation process of the L1 signal at the bottom of occultation (Schreiner et al. 2011). After selecting successfully retrieved GPS-RO events in the three datasets, the total number of profiles available for comparison was 10,838.

### Radiosondes

The Cooperative Indian Ocean experiment on intraseasonal variability in the year 2011 and the joint project of Dynamics of the Madden–Julian Oscillation (CINDY-DYNAMO 2011) are part of an international collaborative campaign to collect in situ observations in the tropics (Yoneyama et al. 2013; Zhang et al. 2013). This project performed intensive radiosonde observations for about six months from October 1, 2011, to March 31, 2012, providing 7789 radiosonde profiles using Vaisala RS92-SGPD and Meisei RS-06G radiosondes from 19 ground stations spread over 35°E–140°E and 10°S–10°N (Fig. 2). In addition, radiosondes were launched every 3 h during the campaign from three research vessels (R/V): Baruna Jaya, Sagar Kanya and Mirai. The boxes in

**Table 1 Basic characteristics of the three COSMIC GPS-RO retrievals**

Dataset	Organization	Sewing height from GO to WO	Vertical resolution in the UTLS	Analysis period
atmPrf2010 (atmPrf version 2010.2640)	UCAR, CDAAC	Variable between 10 and 20 km	0.1–0.2 km when FSI is applied, otherwise 1.4 km	Sep 1, 2010–Jul 17, 2012
atmPrf2013 (atmPrf version 2013.3520)	UCAR, CDAAC	Fixed at 20 km	Originally 0.1–0.2 km by PM, but smoothed over 0.5 km	Apr 22, 2006–Apr 30, 2014
rishfsi2013	RISH, IUGONET	Fixed at 30 km	0.1–0.2 km by FSI	Apr 22, 2006–March 30, 2017

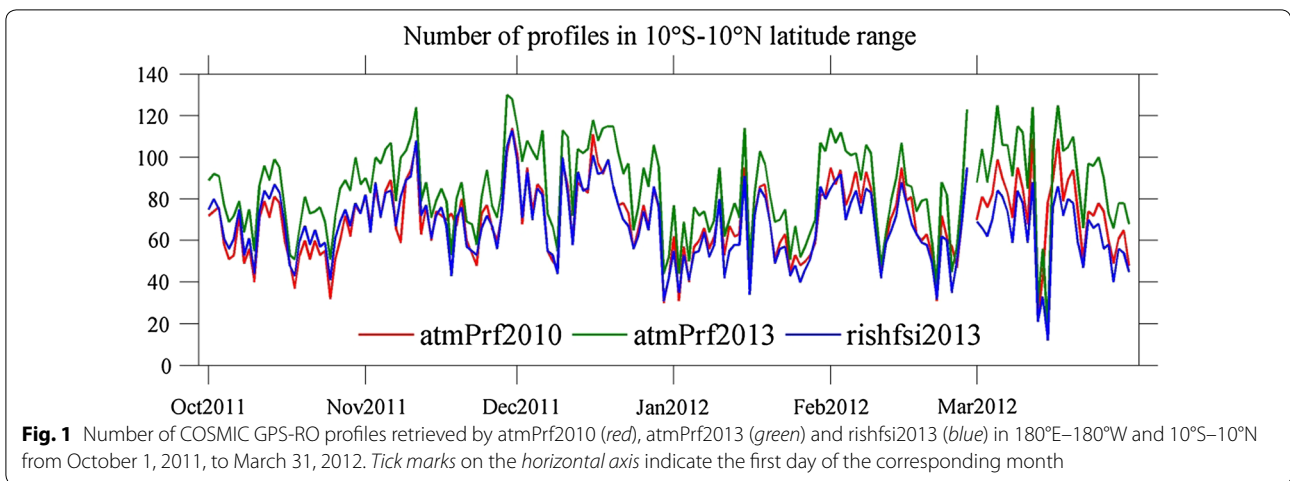
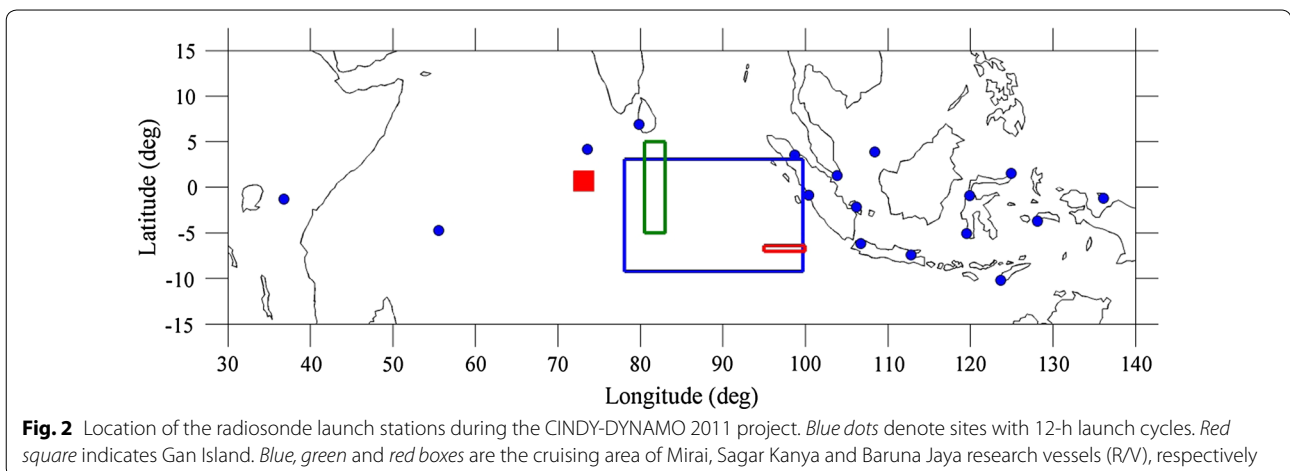


Fig. 2 denote their cruise tracks. The R/V campaigns varied from 3 weeks to 2 months. Moreover, a balloon was launched from Gan Island every 3 h from October 2011 to February 2012. Other ground stations with 12-h routine soundings were located at Seychelles, East of Africa, Nairobi, Maldives, Sri Lanka, Singapore and 13 sites on the Indonesian maritime continents.

The original vertical resolution of the radiosonde data was about 10 m due to the two-second recording intervals. To compare to the COSMIC GPS-RO profiles, the radiosonde data were averaged every 100 m. We selected the COSMIC GPS-RO profiles whose tangent points at a 10-km altitude were within 200 km from the radiosonde sites, and their occultation time was within  $\pm 3$  h from the balloon launch time. We chose the space and time separations for the comparison with radiosondes following the earlier studies (e.g., Kuo et al. 2005; Sun et al. 2010). For the comparison between COSMIC GPS-RO and radiosondes, we found as many as 134 collocated profiles. Note that most of the radiosondes (128 out of

134) were launched during daytime. Hence, a potential difference between day and night launches was difficult to investigate in this study.

Figure 3 shows examples of the  $T$  profiles from the three GPS-RO retrievals and a radiosonde. Two COSMIC GPS-RO events on December 17, 2011, at 22:35:38 UTC (106.24°E, 5.23°S) and 20:18:51 UTC (106.23°E, 5.88°S) occurred nearby the single radiosonde in Cengkareng (Indonesia) at 23:31:00 UTC (106.68°E, 6.12°S). Both atmPrf2013 and atmPrf2010 show smooth data near the tropopause (left profiles), while rishfsi2013 shows detailed temperature variations consistent with the radiosonde result. On the other hand, atmPrf2010 agrees well with rishfsi2013 below 17 km (right profiles), indicating that the sewing height between the GO and WO methods is at 17 km. It is noteworthy that the height resolution of atmPrf2010 near the tropopause depends on the sewing altitude between GO and WO. In contrast, atmPrf2013 always shows a smooth profile up to 20 km. Because rishfsi2013 applies the FSI method up to 30 km,



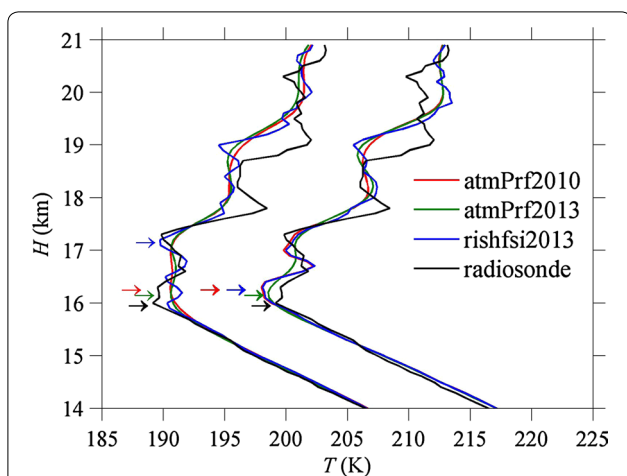


**Fig. 3** Comparison of the  $T$  profiles on December 17, 2011, between the radiosonde at Cengkareng (black line) and two nearby COSMIC GPS-RO by atmPrf2010 (red line), atmPrf2013 (green line) and rishfsi2013 (blue line), respectively. Arrows indicate the CPT altitude of each profile. Profiles on the right are shifted by 10 K

these data provide details of the  $T$  fluctuations in the entire height range.

We defined CPT as the coldest level in the 14- to 20-km altitude. If more than two CPTs were identified, then the CPT height was determined by averaging all the corresponding altitudes. Following the WMO definition, we defined the LRT at the lowest level where the temperature lapse rate ( $-dT/dz$ ) decreases to 2 K/km and the average of the lapse rate between this and higher levels within 2 km does not exceed 2 K/km. We applied the five-point center differential formula to derive  $dT/dz$ . The mean and standard deviation of CPT and LRT from all COSMIC profiles are  $189.5 \text{ K} \pm 1.65 \text{ K}$  at  $17.2 \text{ km} \pm 0.3 \text{ km}$  and  $191.2 \text{ K} \pm 1.55 \text{ K}$  at  $16.4 \text{ km} \pm 0.3 \text{ km}$ , respectively.

### Results and discussion

We investigated the characteristics of the three retrievals of COSMIC GPS-RO, concentrating on the temperature variations in the UTLS region in the tropics by comparing the three retrievals and subsequently validating them using simultaneous radiosonde data.

#### Comparison among the three retrievals

Figure 4 plots the mean and standard deviation of the difference of  $T$  ( $\Delta T$ ) among rishfsi2013, atmPrf2013 and atmPrf2010 at 14- to 21-km altitudes. We limited the lowest height at 14 km, because the dry temperature may become unrealistic due to the effects of the high humidity in the tropics. We also did not show the comparison above 20 km, because the focus of this study is the temperature variations in the UTLS region centered

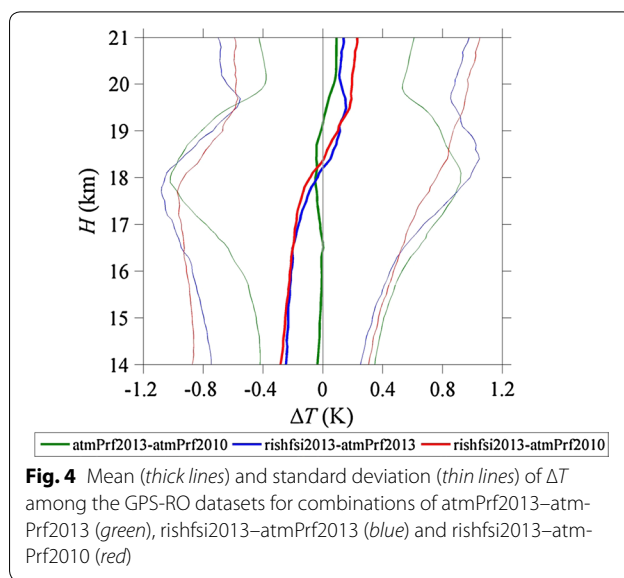


**Fig. 4** Mean (thick lines) and standard deviation (thin lines) of  $\Delta T$  among the GPS-RO datasets for combinations of atmPrf2013–atmPrf2010 (green), rishfsi2013–atmPrf2013 (blue) and rishfsi2013–atmPrf2010 (red)

by the tropopause. Below 19 km, the mean  $\Delta T$  between atmPrf2013 and atmPrf2010 is very small. Above 19 km, it is 0.1 K, at most. The interval of the standard deviation divided by the square root of the number of profiles, which is defined as the standard error of the mean from all  $\Delta T$ , ranges between  $3.7 \times 10^{-3}$  and  $9.8 \times 10^{-3}$  K. Although the standard deviation below 16 km or above 19.5 km ranges 0.3–0.5 K, it is larger at 16–19 km around CPT.

The other two combinations (rishfsi2013–atmPrf2013 and rishfsi2013–atmPrf2010) show similar differences (Fig. 4). The mean  $\Delta T$  at 14 km is  $-0.3 \text{ K}$ , but gradually decreases with height; above 18.5 km, it becomes positive. We applied smoothing over 500 m to the rishfsi2013 profiles and calculated the mean and standard deviation of  $\Delta T$  between the smoothed rishfsi2013 and atmPrf2013 (figure is not shown). The mean  $\Delta T$  shows smaller values (about 0.1 K) than the mean  $\Delta T$  for the rishfsi2013–atmPrf2013 comparison around the tropopause. The standard deviation around the tropopause is reduced from 1.2 to 0.8 K. Hence, the smoothing process to the rishfsi2013 may affect the mean  $\Delta T$  around the tropopause only ( $\sim 0.1 \text{ K}$ ), and it reduces the standard deviation.

We extended the comparison among the three GPS-RO datasets up to 30-km altitude considering the top height of WO used in rishfsi2013 is 30 km (figure is not shown). The atmPrf2013 became gradually warmer than atmPrf2010, and the difference became as large as 0.5 K at 30 km. The rishfsi2013 is warmer than both atmPrf2013 and atmPrf2010 by about 0.1–0.3 K and 0.2–0.5 K at 20–30 km, respectively. The difference above 20 km was in general larger for atmPrf2010 than atmPrf2013 by a factor of about 2. The standard deviation from all

combinations of GPS-RO datasets ranged 0.5–0.8 K at 20 km, and it increased to 1.0–1.5 K above 25 km. The difference between the rishfsi2013 and the two CDAAC versions may be related to the differences in the raw and smoothed atmospheric excess phase.

Considering the increase in the standard deviation of  $\Delta T$  around the tropopause in Fig. 4, we investigated  $\Delta T$  in more detail at both CPT and LRT. Figure 5a shows the daily mean time series of the difference of CPT temperature ( $\Delta T_{CPT}$ ) and the difference of the corresponding altitude ( $\Delta H_{CPT}$ ). Table 2 shows the mean, median and standard deviation of  $\Delta T_{CPT}$  and  $\Delta H_{CPT}$ . The mean  $\Delta T_{CPT}$  is negative for rishfsi2013–atmPrf2013 and rishfsi2013–atmPrf2010, indicating that  $T_{CPT}$  of rishfsi2013 is generally colder than both atmPrf2013 and atmPrf2010. After January 2012, the daily mean  $\Delta T_{CPT}$ 's of both rishfsi2013–atmPrf2013 and rishfsi2013–atmPrf2010 display similar variations. Consequently,  $\Delta T_{CPT}$  for atmPrf2013–atmPrf2010 is close to zero.  $\Delta H_{CPT}$ 's for the three pairs in Fig. 5b show short irregular variations.

$\Delta H_{CPT}$  between the RISH and CDAAC datasets shows a small positive value. However, this result may be insignificant because the difference is within the standard deviation. Therefore, all three datasets are consistent when determining  $H_{CPT}$ .

Figure 6 and Table 3 describe the time series of the daily mean  $\Delta T_{LRT}$  and  $\Delta H_{LRT}$  as well as their statistical results. The magnitudes of the mean  $\Delta T_{LRT}$  for all comparisons are less than 0.6 K, and the standard deviations do not exceed 0.3 K. The mean  $\Delta H_{LRT}$  between rishfsi2013 and atmPrf2013 or atmPrf2010 shows a negative value, whereas the mean  $\Delta H_{LRT}$  between atmPrf2013 and atmPrf2010 is slightly positive. The RISH and CDAAC data produce different behaviors between the temperature and the altitude of CPT and LRT. The mean  $T_{CPT}$  of rishfsi2013 is colder than the two CDAAC products. On the other hand, the mean  $T_{LRT}$  shows the opposite relation. Although the height differences of CPT and LRT are nearly zero, their signs are positive for CPT and negative for LRT.

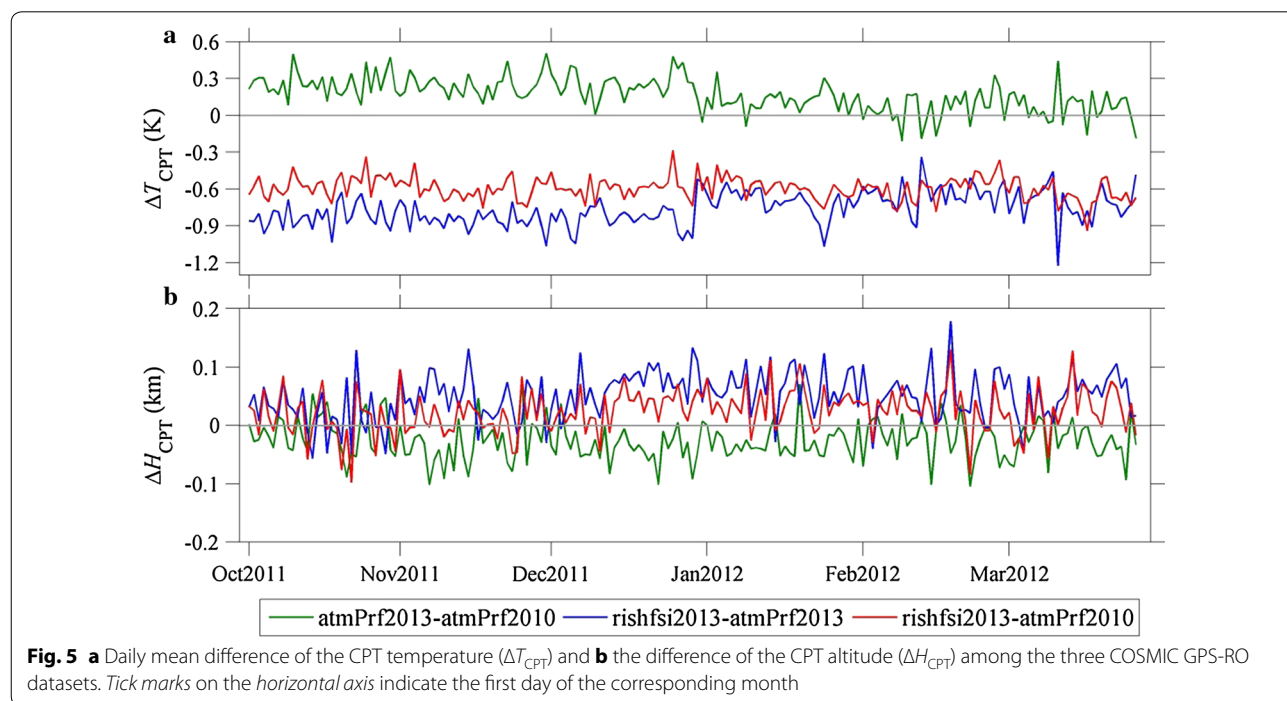


**Fig. 5** **a** Daily mean difference of the CPT temperature ( $\Delta T_{CPT}$ ) and **b** the difference of the CPT altitude ( $\Delta H_{CPT}$ ) among the three COSMIC GPS-RO datasets. Tick marks on the horizontal axis indicate the first day of the corresponding month

**Table 2** Statistical differences of CPT among the three GPS-RO datasets

	$\Delta T$ (K)			$\Delta H$ (km)		
	Mean	Median	Standard deviation	Mean	Median	Standard deviation
atmPrf2013–atmPrf2010	0.17	0.17	0.14	–0.03	–0.03	0.03
rishfsi2013–atmPrf2013	–0.77	–0.77	0.13	0.05	0.05	0.04
rishfsi2013–atmPrf2010	–0.60	–0.59	0.09	0.02	0.03	0.04

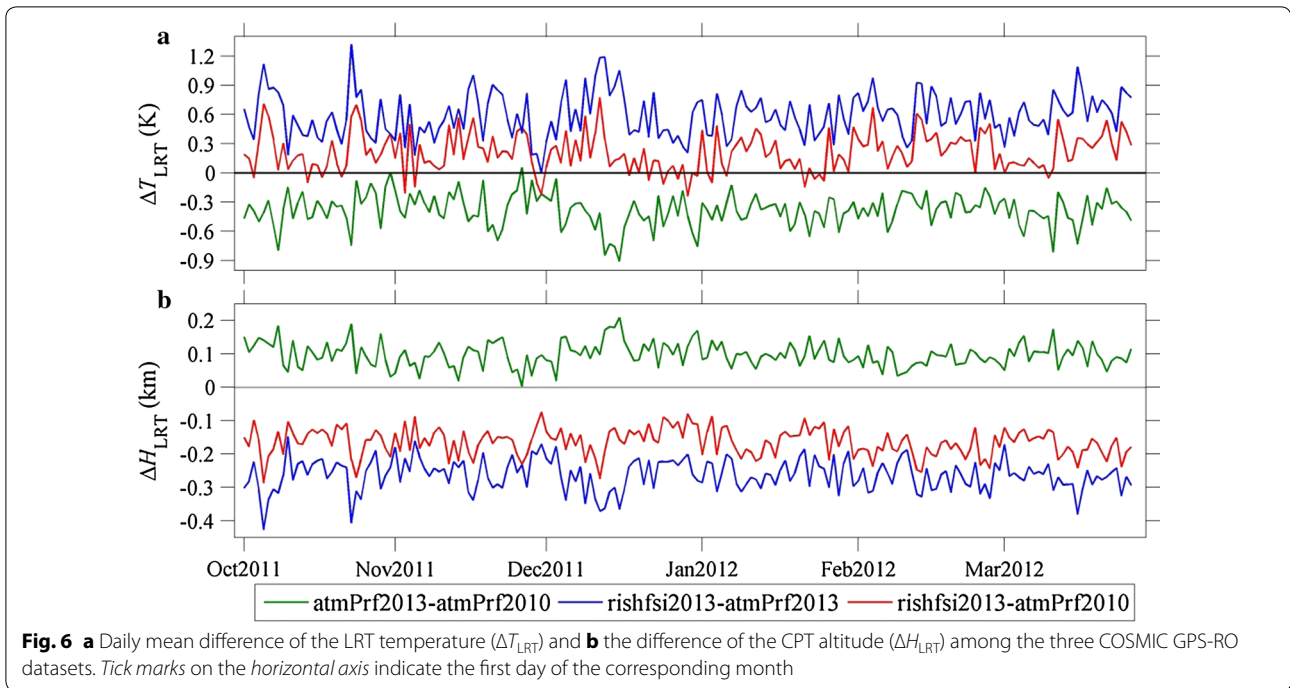


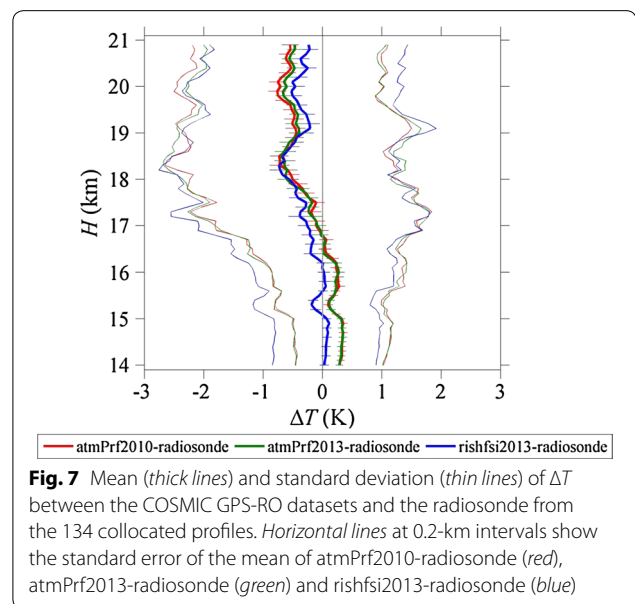
**Table 3** Statistical differences of LRT among the three GPS-RO datasets

	$\Delta T$ (K)			$\Delta H$ (km)		
	Mean	Median	Standard deviation	Mean	Median	Standard deviation
atmPrf2013-atmPrf2010	-0.38	-0.38	0.16	0.09	0.09	0.04
rishfsi2013-atmPrf2013	0.59	0.59	0.22	-0.26	-0.26	0.05
rishfsi2013-atmPrf2010	0.20	0.18	0.20	-0.16	-0.16	0.04

We are interested in differences of the raw bending angles between the RISH and the CDAAC products. A comparison of the optimized bending angles among the three retrievals shows that rishfsi2013 has higher vertical resolution around the tropopause (figure is not shown). These variations seem to be attributed to the background atmospheric model used to optimize the bending angles or the difference in the vertical resolution due to sewing and smoothing. In the next subsection, we compare these GPS-RO data with simultaneous radiosondes to ascertain which products are closer to the real atmosphere.

**Comparison between three COSMIC GPS-RO datasets and Radiosondes**

Because radiosondes are considered as the standard measurement method of temperature, they are compared with the GPS-RO profiles. Figure 7 shows the mean, the standard error of the mean and the standard deviation of  $\Delta T$  between the three GPS-RO retrievals and the



collocated radiosonde profiles. In the entire height range, the average profiles of  $\Delta T$  show similar variations, and the standard error of the mean ranges between 0.06 and 0.18 K. The rishfsi2013 agrees well with the radiosonde at altitudes of 14–16 km, except at 15 km. On the other hand, both atmPrf2013 and atmPrf2010 have positive biases of about 0.2 K. The three GPS-RO results have negative biases of 0.3–0.8 K above LRT, which exists at 16.4 km.

The standard deviation is 1–1.5 K in the troposphere, but increases to about 2 K above the tropopause. The accuracy of temperature measurement with a radiosonde was conducted in the last decades (e.g., Kitchen 1989). Sofieva et al. (2008) showed that the standard deviation of temperature difference among radiosonde profiles obtained within 3 h and 200 km separation was 1 K at 15- to 20-km altitudes. Our result is consistent with this evaluation. Larger deviations in the lower stratosphere are attributed to the effects of the spatial and the temporal variabilities caused by atmospheric

waves (Scherllin-Pirscher et al. 2017; Suzuki et al. 2013).

We compared the atmPrf2013 with the radiosonde results after the 500 m smoothing (figure is not shown). The two comparisons, (atmPrf2013–radiosonde) and (atmPrf2013–smoothed\_radiosonde), are nearly overlapping, and the difference between the two mean  $\Delta T$  profiles ranges from  $-0.1$  to  $0.1$  K. The standard deviation becomes smaller as 0.2 K above the tropopause. Therefore, the smoothing process to the high vertical resolution  $T$  profiles seems to reduce only the standard deviation.

Figure 8 plots the time variations of  $\Delta T_{\text{CPT}}$  and  $\Delta H_{\text{CPT}}$ , while their statistical results are summarized in Table 4. The mean  $\Delta T_{\text{CPT}}$  ranges within  $\pm 0.4$  K, and its standard deviation is about 1.6 K. Although rishfsi2013 shows a colder temperature than the radiosonde, the CDAAC datasets are warmer. The mean of  $\Delta H_{\text{CPT}}$  for all datasets is less than 0.1 km, and the standard deviation is about 0.5 km, which is consistent with the radiosondes.

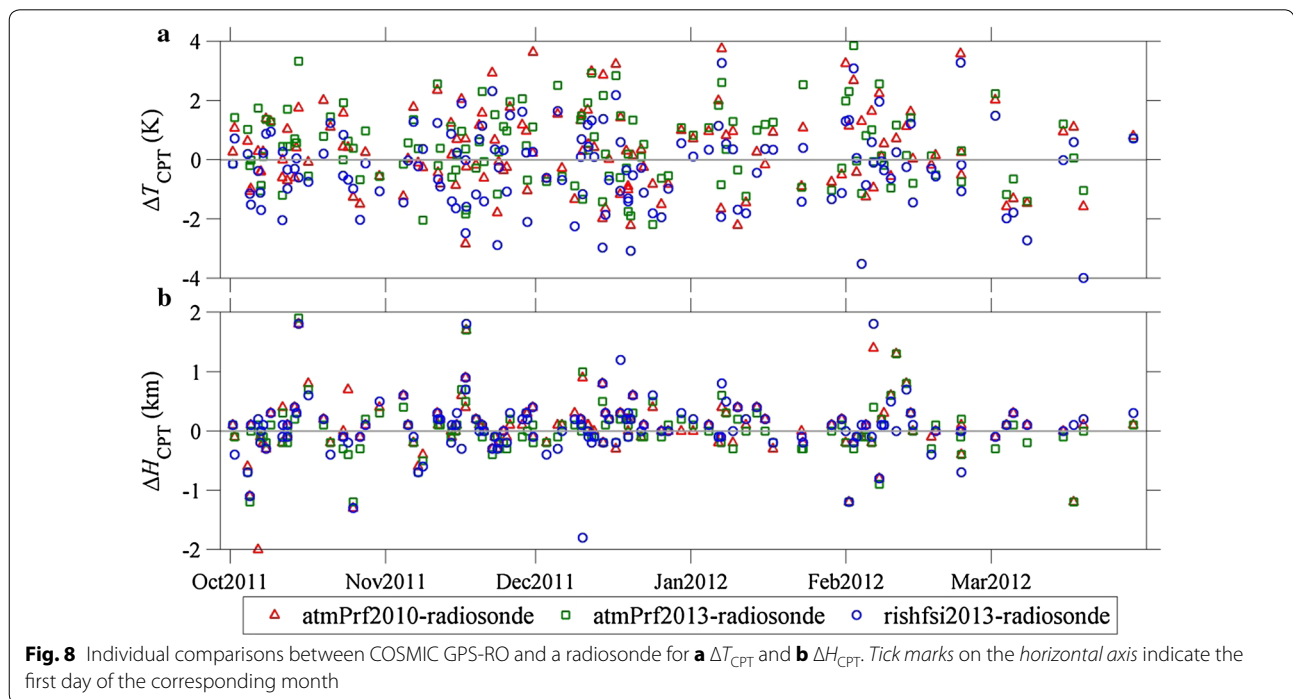


**Table 4** Statistical differences of CPT between GPS-RO and a radiosonde

	$\Delta T$ (K)			$\Delta H$ (km)		
	Mean	Median	Standard deviation	Mean	Median	Standard deviation
rishfsi2013–radiosonde	−0.24	−0.23	1.38	0.07	0.10	0.48
atmPrf2013–radiosonde	0.49	0.38	1.34	0.02	0.00	0.43
atmPrf2010–radiosonde	0.32	0.25	1.33	0.08	0.10	0.48

The  $T$  profiles with the radiosondes and the FSI retrieval have good vertical resolutions, suggesting that they are sensitive to small vertical scale  $T$  fluctuations. Although the mean  $\Delta T_{\text{CPT}}$  for rishfsi2013 is negative (Table 4), both atmprf2010 and atmprf2013 are positive, indicating that they are warmer than  $T_{\text{CPT}}$  by the radiosondes. It is reasonable that atmPrf2013 shows a positive  $\Delta T_{\text{CPT}}$  because height smoothing reduces the sharp temperature fluctuations. Since atmPrf2010 is retrieved by either FSI or GO, depending on the signal condition, the mean  $\Delta T_{\text{CPT}}$  becomes positive due to the mixing of the low-resolution GO results with the sewing altitude below CPT. It should be noted that the mean  $\Delta T_{\text{CPT}}$  of atmPrf2010 is smaller than atmPrf2013, indicating that the former sometimes provides a sharp temperature around CPT (see Fig. 3).

Large  $T$  perturbations around the tropopause produce multiple minima in the  $T$  profile, which are defined as a multiple tropopause. The small difference of  $T$  at these minima can impact the determination of CPT and the

corresponding altitude,  $H_{\text{CPT}}$ . The left profiles in Fig. 3 show a typical example; the CPT is defined at 16 km with the radiosonde, but is detected at 17.1 km with rishfsi2013, leading to a large  $\Delta H_{\text{CPT}}$ , as shown in Fig. 8b. On the other hand, the example in the right profiles in Fig. 3 shows consistency in determining CPT by the three GPS-RO retrievals and the radiosonde. Therefore, the large standard deviation of  $\Delta H_{\text{CPT}}$  (0.5 km) may be due to the effects of a multiple tropopause when determining the coldest minimum.

The variation of  $\Delta T_{\text{LRT}}$  is more complicated (Fig. 9). Table 5 describes the negative mean  $\Delta T_{\text{LRT}}$  ranging from  $-0.41$  to  $-0.69$  K with a standard deviation of about 2.9 K. The  $\Delta H_{\text{LRT}}$  is positive, indicating that the GPS-RO determined the LRT at altitudes 0.1–0.2 km higher than the radiosonde.

We investigated the correlation between  $\Delta T_{\text{CPT}}$  and  $\Delta H_{\text{CPT}}$  in the scatter diagram in Fig. 10 (top panels). Both variables realize the zero mean and the median, but the distribution shows an uncorrelated pattern.

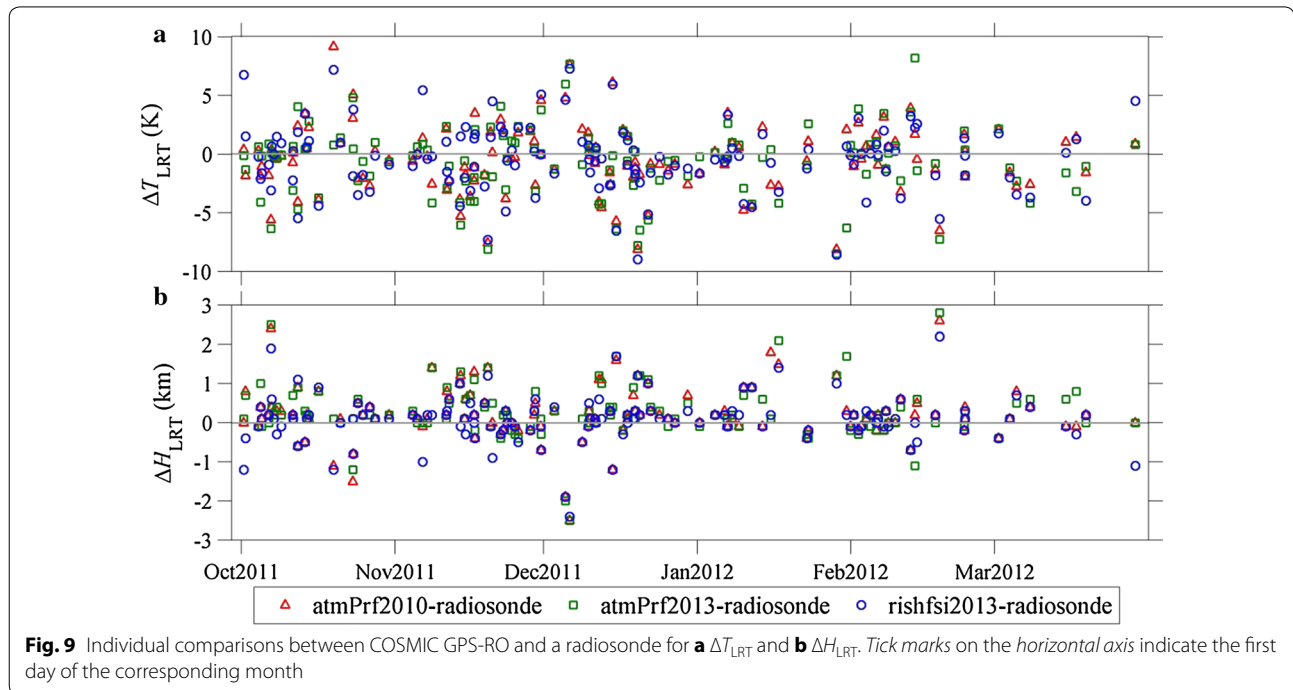


**Fig. 9** Individual comparisons between COSMIC GPS-RO and a radiosonde for **a**  $\Delta T_{\text{LRT}}$  and **b**  $\Delta H_{\text{LRT}}$ . Tick marks on the horizontal axis indicate the first day of the corresponding month

**Table 5** Statistical differences of LRT between GPS-RO and a radiosonde

	$\Delta T$ (K)			$\Delta H$ (km)		
	Mean	Median	Standard deviation	Mean	Median	Standard deviation
rishfsi2013–radiosonde	−0.41	−0.22	2.88	0.09	0.10	0.61
atmPrf2013–radiosonde	−0.69	−0.27	2.91	0.28	0.20	0.67
atmPrf2010–radiosonde	−0.45	−0.40	2.81	0.21	0.20	0.66

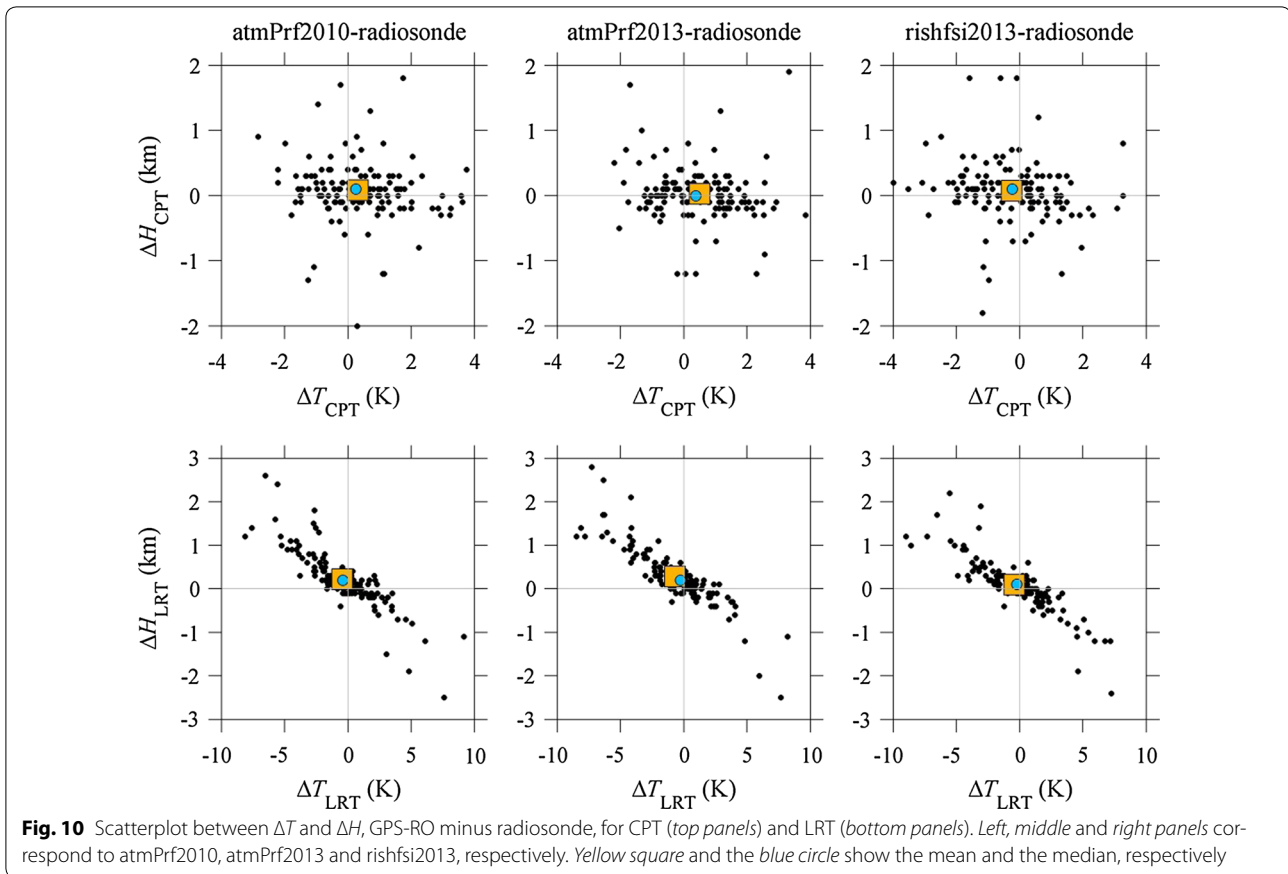
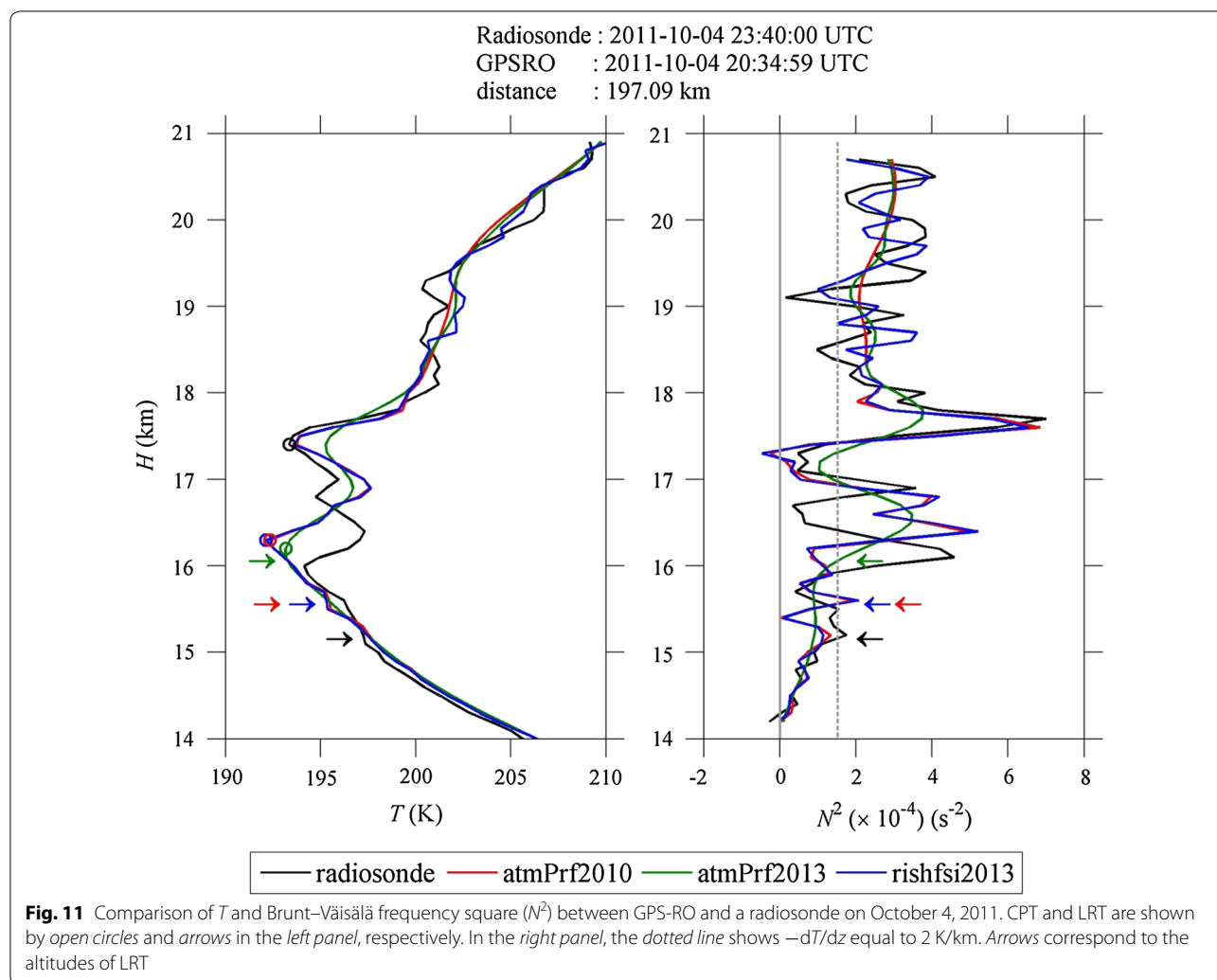


Figure 11 shows an example of the double tropopause near Surabaya, Indonesia, on October 4, 2011. The radiosonde was launched at 23:40:00 UTC (112.78°E, 7.37°S), and the GPS-RO profiles were retrieved at 20:34:59 UTC (111.03°E, 7.11°S). Up to 18.5 km, rishfsi2013 and atmPrf2010 agree well, while atmPrf2013 displays a smooth profile. The temperature at 16–17.5 km shows a large difference, which seems to be attributed to the time and the spatial differences in the temperature field. In some cases in Fig. 10,  $\Delta H_{\text{CPT}}$  becomes as large as  $\pm 2$  km, but the corresponding  $\Delta T_{\text{CPT}}$  is small. The left panel in Fig. 11 shows that the radiosonde identifies the colder  $T_{\text{CPT}}$  at a lower altitude than all the GPS-RO datasets due to the small difference in the individual measurements of  $T_{\text{CPT}}$ . This example indicates that the determination of CPT as the coldest level from the profiles with different height resolutions may produce statistical differences when the multiple tropopause structures frequently appear.

The scatter diagram between  $\Delta T_{\text{LRT}}$  and  $\Delta H_{\text{LRT}}$  in Fig. 10 (bottom panels) shows a linear correlation. Because the LRT is mostly located below the CPT in the equatorial UTLS, the negative (positive)  $\Delta T_{\text{LRT}}$  is associated with the positive (negative)  $\Delta H_{\text{LRT}}$ , resulting in a negative linear tendency. For rishfsi2013 in the leftmost

panel, both positive and negative  $\Delta T_{\text{LRT}}$  are equally distributed. However, an asymmetric distribution is found for atmPrf2010 and atmPrf2013, which have smaller ranges of positive deviations of  $\Delta T_{\text{LRT}}$ . The mean value of  $\Delta H_{\text{LRT}}$  in Table 5 is nearly zero for rishfsi2013, but is as positive as 0.28 and 0.21 km for atmPrf2013 and atmPrf2010, respectively.

The right panel in Fig. 11 shows the Brunt–Väisälä frequency squared ( $N^2$ ). For the radiosonde profile,  $N^2$  exceeds the threshold for LRT at 15.2 km, and the mean stability in the overlying 2-km region satisfies the WMO definition. Consequently, LRT is identified at this altitude. The LRT with rishfsi2013 or atmPrf2010 is similarly determined at 15.6 km. The asymptotic structure of  $N^2$  in Fig. 11 suggests that the actual LRT of these profiles is located around 16–16.5 km, but the enhanced stability at much lower altitudes affects the determination of LRT. On the other hand, atmPrf2013 shows a smooth  $N^2$  profile without an  $N^2$  enhancement at altitudes of 15–16 km. atmPrf2013 identifies the LRT at 16.2 km. We noticed that a profile with a higher vertical resolution is sensitive to a small perturbation of  $N^2$ , which can influence the determination of the appropriate LRT. The smooth profile in atmPrf2013 captures a reliable LRT.



### Discussion

In some cases, the  $T$  profiles show a bias in the UTLS region between atmPrf2010 and atmPrf2013. A typical example is shown in Fig. 12 where the GPS-RO profiles were retrieved at 13:54:58 UTC (118.81°E, 6.30°S) and the radiosonde was launched in Makassar, Indonesia, at 11:30:00 UTC (119.53°E, 5.06°S) on October 19, 2011. The atmPrf2010 profile is warmer than the atmPrf2013 profile by about 2–3 K in the entire height range. CPT is located at 16.5–17.0 km for all the profiles (Fig. 12). Below CPT, the  $T$  profiles from both rishfsi2013 and atmPrf2013 agree well with the radiosonde. However, the radiosonde profile approaches the atmPrf2010 profile above CPT up to about 18.5 km.

The altitudes of CPT and LRT are nearly equal for the radiosonde and atmPrf2013. The LRT altitudes for atmPrf2010 and rishfsi2013 are found around 15.5 km, which is about 1.5 km lower than the other two profiles. The FSI retrieval was applied to both rishfsi2013 and atmPrf2010,

where the sewing height was 19.5 km for atmPrf2010. Between these two retrievals, the  $dT/dz$  profile in the right panel of Fig. 12 agrees very well at 15- to 19.5-km altitudes, suggesting that they capture the  $T$  perturbations identically. However, the  $T$  profiles show a constant bias between rishfsi2013 and atmPrf2010.

This discrepancy may be caused by the difference in the extrapolation height of the ionospheric correction or the difference in the bending angle optimization (Sokolovskiy: personal communication, 2017). We found similar cases in about 10% of the 134 collocated profiles. The differences between the two CDAAC products shown in Fig. 12 may be an unusual case because the statistical results in Fig. 7 show a very good agreement between atmPrf2010 and atmPrf2013.

The example in Fig. 11 indicates that the two versions of the CDAAC products have some discrepancies when determining the altitudes of CPT and LRT, resulting in inconsistencies of the corresponding CPT and

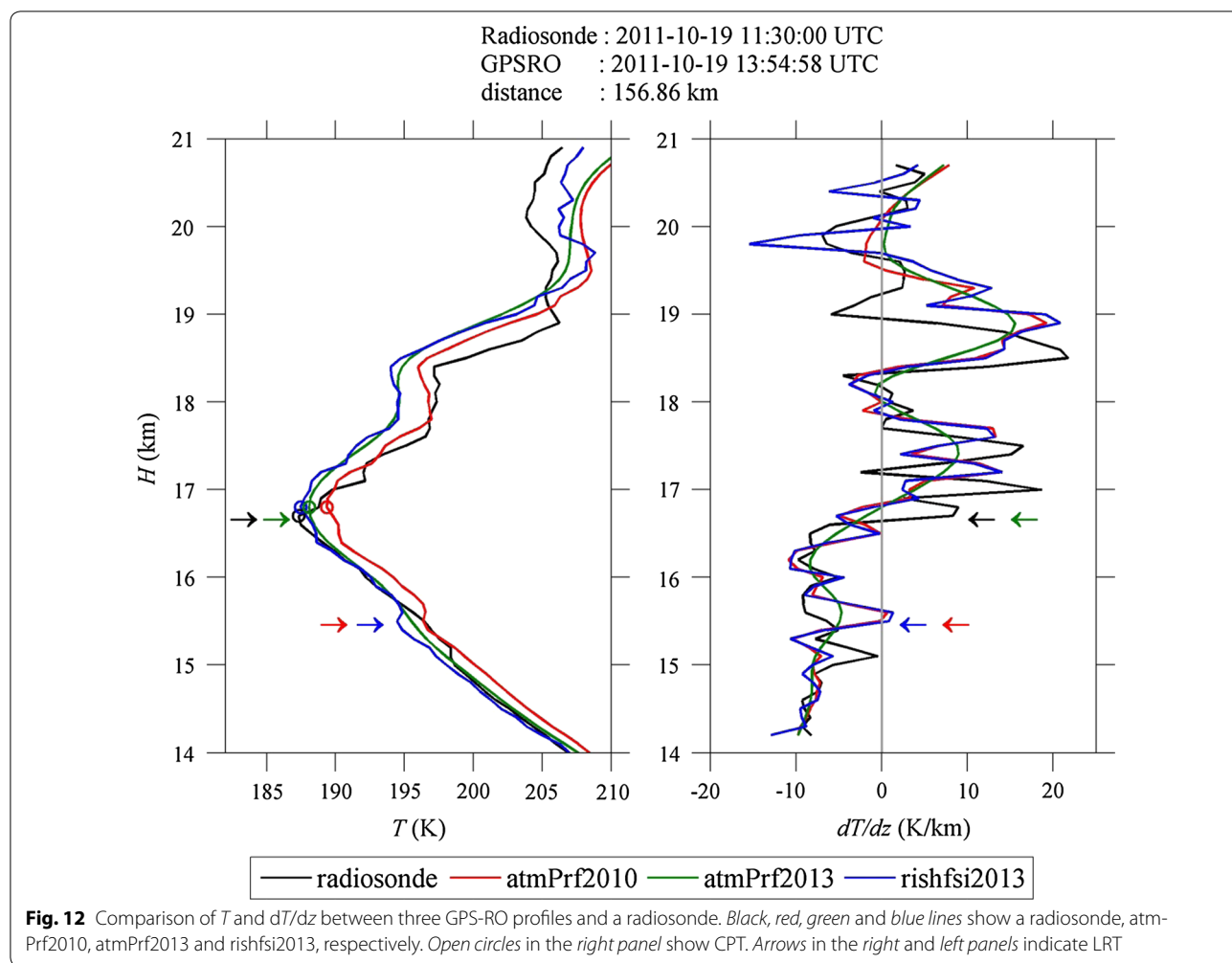


**Fig. 12** Comparison of  $T$  and  $dT/dz$  between three GPS-RO profiles and a radiosonde. Black, red, green and blue lines show a radiosonde, atmPrf2010, atmPrf2013 and rishfsi2013, respectively. Open circles in the right panel show CPT. Arrows in the right and left panels indicate LRT

LRT temperatures. Consequently, statistical analysis of the UTLS parameters should take such differences into account. The background model of climatology utilized in retrieving GPS-RO profiles and the assumptions of the linear combination between L1 and L2 bending angles may control the apparent diversity between the three GPS-RO profiles in Fig. 12 (Schreiner et al. 2011; Zeng et al. 2016).

We examined the  $T$  fluctuations retrieved by the three GPS-RO datasets from individual comparisons (Fig. 12). The power spectral density of  $dT/dz$  (in  $K^2/km$ ) is calculated as a function of the wavenumber (in cycle per kilometer) (Fig. 13). It should be noted that the first point in the spectra is affected by the Hanning window. At large wave numbers between 1.8 and 4.4 cycle/km, rishfsi2013, atmPrf2010 and the radiosonde show a large spectral density (i.e., 0.56–0.23 km in the corresponding wavelength) compared to the spectrum for atmPrf2013. This result confirms the smoothing of the atmPrf2013 profiles for wavelengths shorter than about 500 m, while

atmPrf2010 and rishfsi2013 provide  $T$  profiles with the similar height resolutions as the radiosonde.

### Conclusions

The dry atmospheric temperature ( $T$ ) profiles were retrieved using both GO and WO at CDAAC, which are called atmPrf2010 and atmPrf2013, as well as another dataset at RISH named rishfsi2013. We investigated the  $T$  profiles collected from October 1, 2011, to March 31, 2012, when CINDY-DYNAMO 2011 was conducted.

Firstly, we compared the three GPS-RO retrievals, focusing on the  $T$  differences ( $\Delta T$ ) in the tropical UTLS. The results of combining these three datasets, atmPrf2013–atmPrf2010, rishfsi2013–atmPrf2013 and rishfsi2013–atmPrf2010, are summarized below:

1. The mean  $\Delta T$  between atmPrf2013 and atmPrf2010 is nearly zero, while rishfsi2013 has a slightly negative (positive) bias below (above) the tropopause. All  $\Delta T$  describe the large standard deviation around CPT.

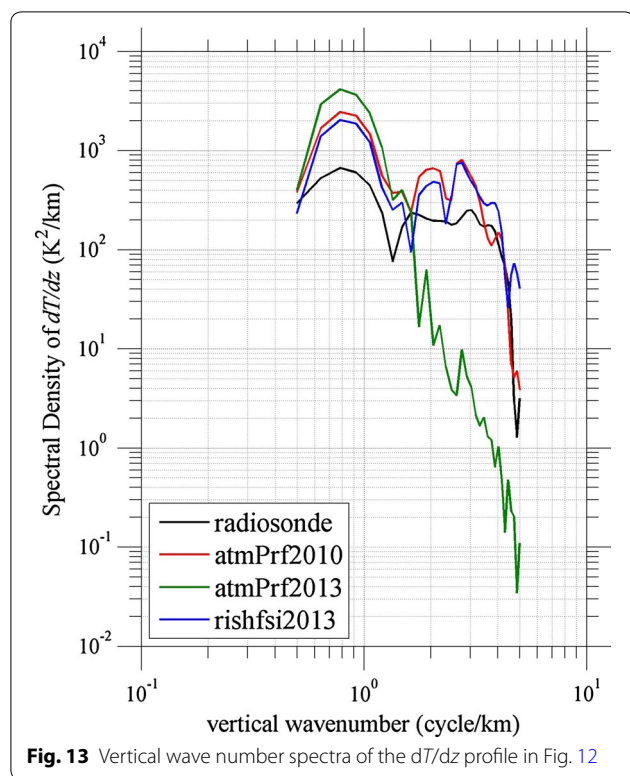


**Fig. 13** Vertical wave number spectra of the  $dT/dz$  profile in Fig. 12

- The mean values of  $\Delta T_{\text{CPT}}$  and  $\Delta T_{\text{LRT}}$  in all comparisons are less than 0.8 and 0.6 K, respectively, with a standard deviation  $<0.3$  K. The rishfsi2013 results indicate a colder (higher)  $T_{\text{CPT}}$  ( $H_{\text{CPT}}$ ) and warmer (lower)  $T_{\text{LRT}}$  ( $H_{\text{LRT}}$ ).
- The discrepancies appear to be due to the difference in the background atmospheric models used for the ionospheric calibration or the difference in the vertical resolution due to sewing and smoothing.

Secondly, we further analyzed  $\Delta T$  between the three GPS-RO retrievals and 134 radiosonde profiles that are within 200 km and  $\pm 3$  h.

- Below LRT, rishfsi2013 agrees with the radiosonde, while both atmPrf2013 and atmPrf2010 indicate a positive bias of 0.2 K. All GPS-RO datasets have a negative bias of 1.0–1.5 K with a standard deviation of about 2 K in the lower stratosphere, which may be attributed to the spatial and temporal variations by the atmospheric waves.
- The mean values of  $\Delta T_{\text{CPT}}$  and  $\Delta H_{\text{CPT}}$  indicate that the three retrievals are consistent with the radiosondes.  $T_{\text{CPT}}$  of rishfsi2013 is colder, while that of the CDAAC profiles is warmer than the radiosonde within  $\pm 0.4$  K. The different height resolutions in

each retrieval influence the determination of CPT when a multiple tropopause appears.

- The scatter diagram between  $\Delta T_{\text{LRT}}$  and  $\Delta H_{\text{LRT}}$  indicates a negative linear tendency. The superior vertical resolution in the radiosonde, rishfsi2013 and atmPrf2010 when the sewing height is detected above the tropopause is sensitive to small-scale  $dT/dz$  perturbations. These fluctuations affect the determination of a reliable LRT; LRT is detected at a lower altitude and a warmer temperature. The smooth atmPrf2013 is more suitable to define LRT.
- The vertical wave number spectral density of  $dT/dz$  is consistent between the rishfsi2013 and the radiosonde in a vertical wave number range larger than 2 cycle/km (wavelength  $< 0.5$  km). However, the spectral density for atmPrf2013 is much smaller due to smoothing.

The statistical results of CPT and LRT agreed relatively well among the three retrievals, although individual profiles sometimes showed considerable discrepancies in the CPT and LRT altitudes due to the multiple tropopause and the height structure of  $dT/dz$ . It is noteworthy that the atmPrf2010 dataset is a mixture of high and low vertical resolutions in the UTLS, depending on the sewing height for individual profiles. Therefore, one may need to pay attention when analyzing the details of tropopause structure related to the  $dT/dz$ , such as the tropopause sharpness (Kim and Son 2012). The  $T$  profiles of atmPrf2013 are useful for climatological analysis of UTLS, although they may not capture the fine structure of the tropopause because of the smoothing over 500 m.

Comparison of rishfsi2013 with the CDAAC products and radiosondes confirm its validity. The  $T$  profiles by rishfsi2013 provide a superior vertical resolution as good as 0.1 km throughout the UTLS region. Thus, rishfsi2013 is useful for studies on the  $T$  fluctuations around the tropopause as well as the behavior of the atmospheric gravity waves in the stratosphere. We encourage the international scientific communities to utilize rishfsi2013, which is now available via the IUGONET system (<http://www.iugonet.org>).

#### Abbreviations

COSMIC: Constellation Observing System for Meteorology, Ionosphere, and Climate; CDAAC: COSMIC data analysis and archive center; IUGONET: Inter-university upper atmosphere global observation NETwork; CPT: cold-point tropopause; LRT: lapse rate tropopause.

#### Authors' contributions

The author N analyzed the data, created the figures and wrote the paper. TT contributed to the manuscript in general. Both authors read and approved the final manuscript.

**Author details**

<sup>1</sup> Research Institute for Sustainable Humanosphere (RISH), Kyoto University, Kyoto, Japan. <sup>2</sup> Center of Atmospheric Science and Technology, National Institute of Aeronautics and Space (LAPAN), Bandung, Indonesia. <sup>3</sup> Research Organization of Information and Systems (ROIS), Tokyo, Japan.

**Acknowledgements**

We acknowledge CDAAC for the use of the COSMIC GPS-RO datasets. We are grateful to Dr. S. Sokolovskiy and Dr. Z. Zeng for their valuable suggestions. We also thank Dr. Atsuki Shinbori for registering the RISH COSMIC GPS-RO dataset in the IUGONET system. This work was partially supported by JSPS KAKENHI Grant Number JP15H03724. One of the authors (N) received a scholarship for his Ph.D. from the Program of Research and Innovation in Science and Technology (RISET-Pro), Ministry of Research, Technology and Higher Education (RISTEKDIKT) of Indonesia.

**Competing interests**

The authors declare that they have no competing interests.

**Availability of data and materials**

The atmPrf version 2010.2640 (atmPrf2010) and 2013.3520 (atmPrf2013) are available at the CDAAC (<http://www.cosmic.ucar.edu>). The rishfsj2013 dataset can be found via <http://search.iugonet.org/list.jsp> (IUGONET), which is formatted in the NetCDF file named as RISHANA\_YYYY.DDD.nc, where YYYY and DDD are the year and Julian day, respectively. The radiosonde data from the CINDY-DYNAMO 2011 are provided by the Japan Agency for Marine-Earth Science and Technology (JAMSTEC) (<http://www.jamstec.go.jp/iorgc/cindy/>) and Earth Observing Laboratory (EOL) of UCAR ([https://www.eol.ucar.edu/field\\_projects/dynamo](https://www.eol.ucar.edu/field_projects/dynamo)).

**Funding**

This work was partially supported by JSPS KAKENHI Grant Number JP15H03724 and the RISH Kyoto University (Mission 5-3).

**Publisher's Note**

Springer Nature remains neutral with regard to jurisdictional claims in published maps and institutional affiliations.

Received: 22 March 2017 Accepted: 28 August 2017

Published online: 11 September 2017

**References**

- Alexander SP, Tsuda T, Kawatani Y, Takahashi M (2008) Global distribution of atmospheric waves in the equatorial upper troposphere and lower stratosphere region: COSMIC observations of wave mean flow interactions. *J Geophys Res* 113:D24115. doi:10.1029/2008JD010039
- Anthes RA (2011) Exploring earth's atmosphere with radio occultation: contributions to weather, climate and space weather. *Atmos Meas Tech* 4:1077–1103. doi:10.5194/amt-4-1077-2011
- Anthes RA, Ector D, Hunt DC, Kuo YH, Rocken C, Schreiner WS, Sokolovskiy SV, Syndergaard S, Wee TK, Zeng Z, Bernhardt PA, Dymond KF, Chen Y, Liu H, Manning K, Randel WJ, Trenberth KE, Cucurull L, Healy SB, Ho SP, McCormick C, Meehan TK, Thompson DC, Yen NL (2008) The COSMIC/FORMOSAT-3 mission: early results. *B Am Meteorol Soc* 89:313–333
- Das U, Pan CJ (2014) Validation of FORMOSAT-3/COSMIC level 2 "atmPrf" global temperature data in the stratosphere. *Atmos Meas Tech* 7:731–742. doi:10.5194/amt-7-731-2014
- Fueglistaler SA, Dessler E, Dunkerton TJ, Folkins I, Fu Q, Mote PW (2009) The tropical tropopause layer. *Rev Geophys* 47:RG1004. doi:10.1029/2008RG000267
- Gottelman A, Hoor P, Pan LL, Randel WJ, Hegglin MI, Birner T (2011) The extratropical upper troposphere and lower stratosphere. *Rev Geophys* 49:RG3003. doi:10.1029/2011RG0003555
- Gorunov ME (2002) Canonical transform method for processing radio occultation data in the lower troposphere. *Radio Sci* 37(5):1076. doi:10.1029/2000RS002592
- Gorunov ME, Lauritsen KB (2004) Analysis of wave fields by Fourier integral operators and their application for radio occultations. *Radio Sci* 39:RS4010. doi:10.1029/2003RS002971
- Gubenko VN, Paveleyev AG, Salimzyanov RR, Paveleyev AA (2011) Reconstruction of internal gravity wave parameters from radio occultation retrievals of vertical temperature profiles in the earth's atmosphere. *Atmos Meas Tech* 4:2153–2162. doi:10.5194/amt-4-2153-2011
- Jensen AS, Lohmann MS, Benzon H, Nielsen AS (2003) Full spectrum inversion of radio occultation signals. *Radio Sci* 38(3):1040. doi:10.1029/2002RS002763
- Jensen AS, Lohmann MS, Nielsen AS, Benzon H (2004) Geometrical optics phase matching of radio occultation signals. *Radio Sci* 39:RS3009. doi:10.1029/2003RS002899
- Kim J, Son S-W (2012) Tropical cold-point tropopause: climatology, seasonal cycle and intraseasonal variability derived from COSMIC GPS radio occultation measurements. *J Clim* 25:5343–5360. doi:10.1175/JCLI-D-11-00554.1
- Kitchen M (1989) Representativeness errors for radiosonde observations. *QJR Meteorol Soc* 115:673–700
- Kuo Y-H, Wee TK, Sokolovskiy S, Rocken C, Schreiner W, Hunt D, Anthes RA (2004) Inversion and error estimation of GPS radio occultation data. *J Meteorol Soc Jpn* 82:507–531
- Kuo Y-H, Schreiner WS, Wang J, Rossiter DL, Zhang Y (2005) Comparison of GPS radio occultation soundings with radiosondes. *Geophys Res Lett* 32:L05817. doi:10.1029/2004GL021443
- Kursinski ER, Hajj GA, Schofield JT, Linfield RP, Hardy KR (1997) Observing earth's atmosphere with radio occultation measurements using the global positioning system. *J Geophys Res* 102:23429–23465. doi:10.1029/97JD01569
- Ladstädter F, Steiner AK, Schwärz M, Kirchengast G (2015) Climate intercomparison of GPS radio occultation, RS 90/92 radiosondes and GRUAN from 2002 to 2013. *Atmos Meas Tech* 8:1819–1834. doi:10.5194/amt-8-1819-2015
- Melbourne WG (2004) *Radio occultations using earth satellites*. Wiley, New Jersey
- Scherllin-Pirscher B, Kirchengast G, Steiner AK, Kuo Y-H, Foelsche U (2011) Quantifying uncertainty in climatological fields from GPS radio occultation: an empirical-analytical error model. *Atmos Meas Tech* 4:2019–2034. doi:10.5194/amt-4-2019-2011
- Scherllin-Pirscher B, Randel WJ, Kim J (2017) Tropical temperature variability and Kelvin-wave activity in the UTLS from GPS-RO measurements. *Atmos Chem Phys* 17:793–806. doi:10.5194/acp-17-793-2017
- Schreiner W, Sokolovskiy S, Hunt D, Rocken C, Kuo Y-H (2011) Analysis of GPS radio occultation data from the FORMOSAT-3/COSMIC and Metop/GRAS missions at CDAAC. *Atmos Meas Tech* 4:2255–2272. doi:10.5194/amt-4-2255-2011
- Sofieva VF, Dalaudier FR, Kiwi R, Kyro E (2008) On the variability of temperature profiles in the stratosphere: implications for validation. *Geophys Res Lett* 35:L23808. doi:10.1029/2008GL035539
- Sokolovskiy S, Schreiner W, Rocken C, Hunt D (2009) Optimal noise filtering for the ionospheric correction of GPS radio occultation signals. *J Atmos Ocean Tech* 26:1398–1403
- Sokolovskiy S, Rocken C, Schreiner W, Hunt D (2010) On the uncertainty of radio occultation inversions in the lower troposphere. *J Geophys Res* 115:D22111. doi:10.1029/2010JD014058
- Sokolovskiy SV, Schreiner WS, Zeng Z, Hunt DC, Kuo Y-H, Meehan TK, Stecheson TW, Mannucci AJ, Ao CO (2014) Use of the L2C signal for inversions of GPS radio occultation data in the neutral atmosphere. *GPS Solut* 18:405–416. doi:10.1007/s10291-013-0340-x
- Steiner AK, Lackner BC, Ladstädter F, Scherllin-Pirscher B, Foelsche U, Kirchengast G (2011) GPS radio occultation for climate monitoring and change detection. *Radio Sci* 46:RS0D24. doi:10.1029/2010RS004614
- Sun B, Reale A, Seidel DJ, Hunt DC (2010) Comparing radiosonde and COSMIC atmospheric profile data to quantify differences among radiosonde types and the effects of imperfect collocation on comparison statistics. *J Geophys Res* 115:D23104. doi:10.1029/2010JG014457
- Suzuki J, Fujiwara M, Nishizawa T, Shirooka R, Yoneyama K, Katsumata M, Matsui I, Sugimoto N (2013) The occurrence of cirrus clouds associated with eastward propagating equatorial  $n = 0$  inertia-gravity and Kelvin waves in November 2011 during the CINDY2011/DYNAMO campaign. *J Geophys Res* 118:12941–12947. doi:10.1002/2013JD019960

- Tsuda T, Lin X, Hayashi H, Noersomadi N (2011) Analysis of vertical wave number spectrum of atmospheric gravity waves in the stratosphere using COSMIC GPS radio occultation data. *Atmos Meas Tech* 4:1627–1636. doi:[10.5194/amt-4-1627-2011](https://doi.org/10.5194/amt-4-1627-2011)
- Wang B-R, Liu X-Y, Wang J-K (2013) Assessment of COSMIC radio occultation retrieval product using global radiosonde data. *Atmos Meas Tech* 6:1073–1083. doi:[10.5194/amt-6-1073-2013](https://doi.org/10.5194/amt-6-1073-2013)
- Ware R, Exner M, Feng D, Gorbunov M, Hardy K, Herman B, Kuo Y, Meehan T, Melbourne W, Rocken C, Schreiner W, Sokolovskiy S, Solheim F, Zou AR, Businger S, Trenbeth K (1996) GPS sounding of the atmosphere from low Earth orbit—preliminary results. *Bull Am Meteorol Soc* 77:19–40
- Xu X, Gao P, Zhang X (2014) Global multiple tropopause features derived from COSMIC radio occultation data during 2007 to 2012. *J Geophys Res Atmos* 119:8515–8534. doi:[10.1002/2014JD021620](https://doi.org/10.1002/2014JD021620)
- Yoneyama K, Zhang C, Long CN (2013) Tracking pulses of the Madden–Julian oscillation. *Bull Am Meteorol Soc*. doi:[10.1175/bams-d-12-00157.1](https://doi.org/10.1175/bams-d-12-00157.1)
- Zeng Z, Sokolovskiy S, Schreiner W, Hunt D, Lin J, Kuo Y-H (2016) Ionospheric correction of GPS radio occultation data in the troposphere. *Atmos Meas Tech* 9:335–346. doi:[10.5194/amt-9-335-2016](https://doi.org/10.5194/amt-9-335-2016)
- Zhang C, Gottschalck J, Maloney ED, Moncrieff MW, Vitart F, Waliser DE, Wang B, Wheeler MC (2013) Cracking the MJO nut. *Geophys Res Lett* 40:1223–1230. doi:[10.1002/grl.50244](https://doi.org/10.1002/grl.50244)

**Submit your manuscript to a SpringerOpen<sup>®</sup> journal and benefit from:**

- ▶ Convenient online submission
- ▶ Rigorous peer review
- ▶ Open access: articles freely available online
- ▶ High visibility within the field
- ▶ Retaining the copyright to your article

---

Submit your next manuscript at ▶ [springeropen.com](http://springeropen.com)

---